Effect of C content on microstructure evolution and mechanical properties of $CoCrFeNiTa_{0.1}$ high entropy alloy

Aoxiang Li, Kaiwen Kang, Su Xu, Jinshan Zhang, Di Huang, Chunning. Che, Yaqing Li, Mingkun Xu, Saike Liu, Yiteng Jiang, Gong Li

PII: S0925-8388(24)01725-0

DOI: https://doi.org/10.1016/j.jallcom.2024.175138

Reference: JALCOM175138

To appear in: *Journal of Alloys and Compounds*

Received date: 7 March 2024
Revised date: 24 May 2024
Accepted date: 9 June 2024

Please cite this article as: Aoxiang Li, Kaiwen Kang, Su Xu, Jinshan Zhang, Di Huang, Chunning. Che, Yaqing Li, Mingkun Xu, Saike Liu, Yiteng Jiang and Gong Li, Effect of C content on microstructure evolution and mechanical properties of $CoCrFeNiTa_{0.1}$ high entropy alloy, *Journal of Alloys and Compounds,* (2024) doi:https://doi.org/10.1016/j.jallcom.2024.175138

Effect of C content on microstructure evolution and mechanical properties of $CoCrFeNiTa_{0.1}$ high entropy alloy

Aoxiang Li, Kaiwen Kang, Su Xu, Jinshan Zhang, Di Huang, Chunning. Che, Yaqing Li, Mingkun Xu, Saike Liu, Yiteng Jiang, Gong Li*

State Key Laboratory of Metastable Materials Science and Technology, Yanshan University, Qinhuangdao, 066004, China

**Corresponding authors E-mail address: Gong Li: gongli@ysu.edu.cn;*

Abstract

A series of $CoCrFeNiTa_{0.1}C_x$ (x = 0.1, 0.2, 0.3, 0.4, 0.5) high entropy alloys (HEAs) with different C content were prepared by vacuum melting technology. The influence of different C element contents on the alloy microstructure and mechanical properties have been systematically investigated using X-ray diffraction, scanning electron microscopy, transmission electron microscopy, and a universal testing machine system. It is found that the introduction of trace amounts of C element content facilitates the precipitation of Laves phase in C0.1 alloy. As the C element content further increases, the volume fractions of both FCC matrix and Laves phases gradually decrease, while the volume fraction of M_7C_3 carbide increases. Notably, the $CoCrFeNiTa_{0.1}C_{0.3}$ HEA shows a ternary eutectic structure. Compression tests reveal an increase in yield strength from 342 MPa to 1475 MPa and hardness from 182 HV to 458 HV as the C content increases. The precipitation of Laves phase and M_7C_3 carbide is principally involved in the enhancement of strength and hardness. Nanoindentation tests indicate that the M_7C_3 carbide has a higher nano-hardness compared to FCC matrix and Laves phase. The

fracture microstructure exhibits a mode transition from ductile fracture to cleavage fracture.

Keywords: Composite materials, Microstructure, High entropy alloy, Nano-hardness, Cleavage fracture

1. Introduction

High entropy alloys (HEAs) are defined as a category of alloys consisting of at least four major elements, each of which is present in a molar ratio in the range of 5% to 35% [1-4]. The extensive compositional space of HEAs not only inspires innovative materials design but also offers significant opportunities for tailoring microstructure and properties [5-8]. In particular, face-centered cubic (FCC) HEAs have attracted considerable interest for remarkable ductility at room temperature [9-14]. However, the limited strength of FCC HEAs hampers their application as engineering materials [15-19]. Consequently, improving the strength of FCC HEAs has been an essential focus of the advanced materials research community in recent years. [11, 20-23].

A common method of strengthening is adding interstitial elements like C [24], O [25], and N [26]. For instance, Zhang et al. [27] have produced a series of CoCrFeNiCx HEAs by vacuum arc melting. The results showed that with the C element added to the alloy, a distinctive dendrite structure was observed. Besides, the yield strength increased by approximately 200 MPa at 0.9 wt.% C element content. This strengthening effect is primarily due to solid-solution strengthening induced via interstitial C atoms and precipitation strengthening induced by M_7C_3 carbide (M represents the sum of all metal elements). In another study, Wang et al. [28] designed a near-eutectic $Fe_{2-y}CoNiCr_yC_x$ HEA. The results indicated a transition in alloy microstructure from hypoeutectic to hypereutectic and a shift in the secondary phase from FCC to M_7C_3 carbide with increasing C content. The $Fe_{1.2}CoNiCr_{0.8}C_{0.45}$ HEA exhibited outstanding performance, with a yield strength of 1934 MPa and an elasticity of 21.3%, mainly

owing to the precipitation of dense M_7C_3 carbide. Furthermore, Huang et al. [29] prepared $C_xCoCr_3Fe_5Ni$ HEAs by vacuum melting technology. The results showed that the alloy changes from FCC+BCC biphase structure to FCC+ $M_{23}C_6$ carbide eutectic mixture structure with the increase of C content. Tensile tests showed that the yield strength of C0.2 eutectic HEA increased from 307.5 MPa to 378.9 MPa, ultimate tensile strength from 646.5 MPa to 837.1 MPa, and ductility from 55.4% to 56.1% compared with C0 base alloy. The synergistic strengthening of the strength and ductility was mainly attributed to the combination of solid solution strengthening and eutectic phase strengthening. Klimova [30] studied the effects of different C element contents on the phase composition, microstructure, and mechanical properties of the CoCrFeMnNi HEA during thermomechanical processing. It was found that with the increase of C element content, the material exhibited extremely attractive mechanical property combinations both at room temperature and in low-temperature environments. The interstitial atoms are crucial in the modification of the microstructure and mechanical properties of the HEAs [31, 32]. Therefore, there is a need for investigation of the influence of interstitial atoms in HEAs microstructure and mechanical properties.

In this investigation, a series of $CoCrFeNiTa_{0.1}C_x$ HEAs have been synthesized by incorporation of different amounts of C elements. The microstructure evolution of the alloys was comprehensively investigated. The mechanical properties of alloys containing different contents of C element have been carefully evaluated by compression test and nanoindentation test. This study focuses on the effects of different C contents on the microstructure and mechanical properties of alloys, providing novel

insights for designing advanced HEA systems with innovative structures and excellent properties.

2. Experimental

2.1 Specimen preparation

A series of $CoCrFeNiTa_{0.1}C_x$ (x=0, 0.1, 0.2, 0.3, 0.4, 0.5, where x represents the atomic proportion of C) HEAs were carefully prepared by arc melting a composition of highly pure metal components each exceeding 99.95 wt.%. The process was iteratively performed five times to achieve chemical homogeneity. For precise delineation in discourse, the alloys, distinguished by varying carbon content, are identified as C0, C0.1, C0.2, C0.3, C0.4, and C0.5, respectively.

2.2 Microstructure characterization

The crystallographic phases of the alloy phases were determined by XRD diffraction (D/Max-2500/PCX) with Cu-Kα radiation (λ = 1.54 Å) at the working voltage and current of 60 kV and 300 mA using a 20-100° scan range and a scanning rate of 4 °/min. The morphology of the alloy was characterized by scanning electron microscopy (SEM Hitachi S-3400) at the functioning voltage and current of 15 kV and 40 mA and transmission electron microscopy (TEM-F200X) at the operating voltage of TEM imaging and EDS is 200 kV. For SEM observation, the sample underwent mechanical grinding using sandpaper of varying grit sizes until all discernible scratches were eliminated. Following this, perpendicular mechanical polishing was performed until a mirror-like surface was attained. Subsequently, the polished sample underwent etching with aqua regia (HNO_3:HCl = 1:3). TEM foils are mechanically ground to

approximately 50 μm, punch into a 3 mm diameter round plate, and then thin using twin-jet electro-polishing in a 10 vol.% $HClO_4$ + 90 vol.% CH_3OH solution at -20 ℃ with a 20 V potential. During the statistical process, over five independent sets of data were used for each sample to guarantee the accuracy of the data.

2.3 Mechanical test

Cylindrical compressive samples, exhibiting a ratio of 1:2 (Φ3 × 6 mm), underwent precise sectioning via electrical-discharge machining (EDM). The compression tests of the alloy are tested with a constant strain rate of 0.48 mm/min using an INSTRON-5982 universal tensile machine equipped with a mechanical extension meter. Subsequently, Vickers hardness tests were conducted on the FM-ARS 9000 micro-hardness tester. Three samples were taken from each experiment during the test to ensure the accuracy of the experiment. Nano-indentation testing was performed using Hysitron triboindenters (TI-900) equipped with Berkovich diamond tips and in-situ atomic force microscopy (AFM), with an efficient tip diameter of approximately 450 nm. Preceding the nano-indentation, the specimens underwent grinding with fine SiC abrasive paper, followed by subsequent polishing to achieve a 10 nm mirror finish. The nano-indentation test comprised loading at a rate of 1000 μN/s to 8000 μN, with a 2 s holding period, and the same rate was applied during unloading. To ensure experimental precision, measurements were taken at 20 distinct points for each sample.

3. Result

3.1 Microstructure investigation

Fig. 1 displays the XRD results of $CoCrFeNiTa_{0.1}C_x$ HEAs showing the presence

of FCC matrix, Laves phase, and M_7C_3 carbide. Specifically, only the FCC matrix and Laves phase are present in the C0 alloy. Compared with C0 alloy, C0.1 alloy has a higher Laves phase diffraction peak intensity, suggesting trace C element introduction promotes the precipitation of the Laves phase. With the C element content further increasing, the diffraction peak corresponding to M_7C_3 carbide appears, associated with a gradual decrease in the Laves phase diffraction peak intensity and corresponding increases in the M_7C_3 carbide diffraction peak. In Fig. 1(b), an enlarged image of the (111) diffraction peak shows a significant shift to a lower 2θ angle with increasing C content. For the $CoCrFeNiTa_{0.1}C_x$ HEAs, where the C element serves as a solute element with $CoCrFeNiTa_{0.1}$ as the solvent, the lattice constants of the alloys can be calculated using the following formula [33]:

$$\alpha = \alpha_0 + \sum_{i=1}^{n-1} \frac{d\alpha}{d(c_i - c_0)}(c_i - c_0) \quad (1)$$

where α_0 is the lattice constant of the solvent, c_i represents the concentration of solute i, $\frac{d\alpha}{dc}$ is the coefficient of lattice parameter change for the corresponding solute, $(c_i - c_0)$ is the deviation from the reference composition, and $\frac{d\alpha}{d(c_i - c_0)}$ is assumed to be constant in a finite range. Therefore, the lattice constants of alloys C0.1, C0.2, C0.3, C0.4, and C0.5 are calculated to be 0.3584 nm, 0.3588 nm, 0.3589 nm, 0.3593 nm, and 0.3594 nm, respectively. The C atoms exist in the interstitial form within the FCC lattice, and as the C content increases, promoting the slightly increased solid solubility of C atoms leads to an increase in lattice distortion. In addition, as the C element content increases, the FCC diffraction peak intensity gradually decreases caused by the increasing volume fraction of M_7C_3 carbide.

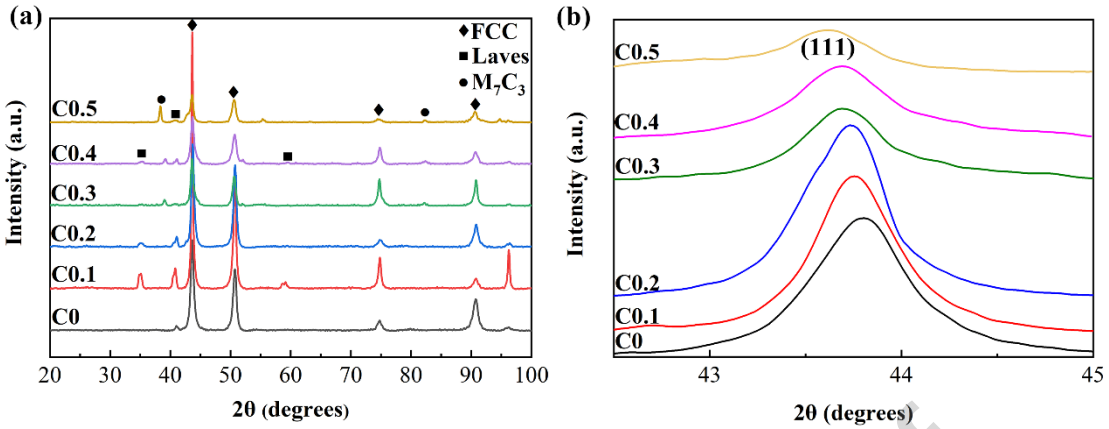

Fig. 1. The crystallographic phases of $CoCrFeNiTa_{0.1}C_x$ HEAs. (a) The XRD results of HEAs. (b) Magnified image of the (111) diffraction peak.

Fig. 2 illustrates the microstructure of CoCrFeNiTa0.1Cx HEAs. Each alloy exhibits a typical dendritic (DR) structure. Figs. 2(a-a_1) shows the C0 alloy with alternating streaks of light and dark distribution. Previous studies have identified dark regions as FCC phases and light regions as Laves [34], aligning with the XRD results. In comparison, Figs. 2(b-b_1) displays that C0.1 alloys have a higher Laves phase content, suggesting that the introduction of C elements promotes the precipitation of the Laves phase, forming a eutectic structure in the interdendritic (ID) region. The eutectic structure of the Laves phase is due to the higher affinity between Ta and C elements than other metal elements in the alloy. Figs. 2(c-c_1) indicates that in addition to the Laves phase, traces of black rod-like M_7C_3 carbide are observed within the ID region of C0.2 alloy, and the Laves phase volume fraction is reduced compared to the C0.1 alloy. As the C element content is further increased, the content of rod-like carbide gradually increases while the content of the Laves phase decreases. Notably, a ternary eutectic structure is formed between the dendrites of the C0.3 alloy. The C0.5 alloy exhibits an abundance of rod-like carbides with only traces of Laves phases remaining

as shown in Figs. 2(f-f$_1$). Table 1 presents the volume fraction of individual phases in CoCrFeNiTa$_{0.1}$C$_x$ HEAs as measured by Image-J software. With increasing C element content, the volume fraction of Laves phase initially increases and then decreases, while the M_7C_3 carbide volume fraction gradually increases. In particular, M_7C_3 carbide appears in the alloy and its volume fraction gradually increases as the volume fraction of the Laves phase initially decreases. This indicates that a high content of C element will inhibit the generation of the Laves phase and will facilitate the formation of the M_7C_3 carbide.

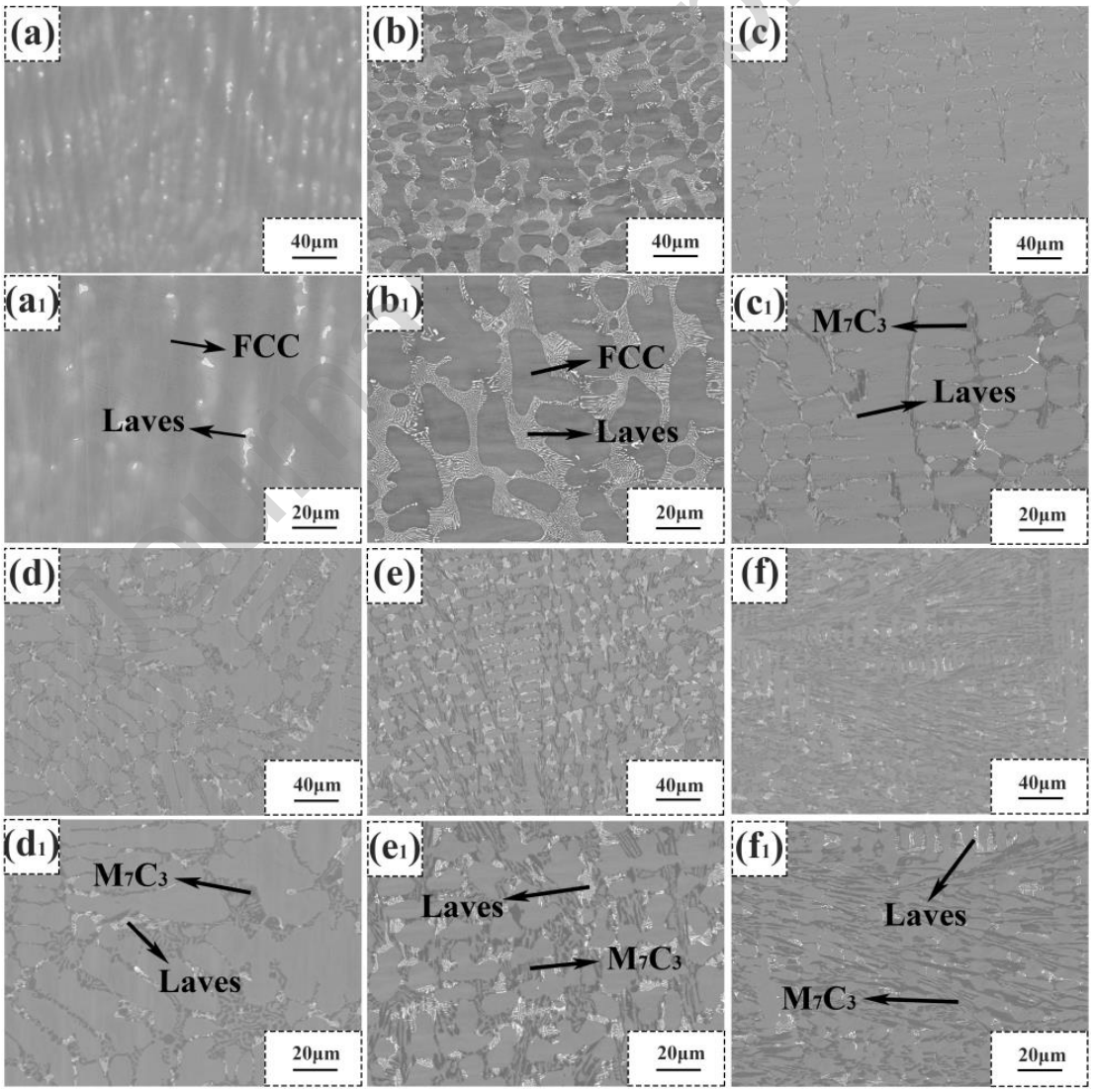

Fig. 2. SEM results of the C0 (a-a_1), C0.1 (b-b_1), C0.2 (c-c_1), C0.3 (d-d_1), C0.4 (e-e_1) and C0.5 (f-f_1) alloys.

Table 1. The volume fraction of each individual phase within $CoCrFeNiTa_{0.1}C_x$ HEAs

	C0	C0.1	C0.2	C0.3	C0.4	C0.5
FCC	99.03	83.43	87.72	81.61	70.74	57.06
Laves	0.97	16.57	5.86	4.26	3.85	1.78
M_7C_3	-	-	6.42	14.13	25.41	41.61

TEM analysis was performed for further structural characterization of the C0.1, C0.2 and C0.3 alloys. Fig. 3(a) displays a significant layer precipitate presence in the C0.1 alloy with a length of ~15 μm and a width of ~0.1 μm. The corresponding SAED pattern confirms that these layered precipitates are Laves phases with hexagonal close-packed structures. In addition, eutectic structures with an average distance of 0.5 μm are formed within the ID region, indicating that the C0.1 alloy has a typical hypoeutectic structure. Fig. 4 presents the results of the qualitative chemical analysis of the C0.1 alloy, demonstrating the uniform distribution of Co, Cr, Fe, and Ni in the FCC matrix, while Ta and C are enriched in the Laves phase. The elemental contents of the individual phases within the C0.1 alloy are specified in Table 2.

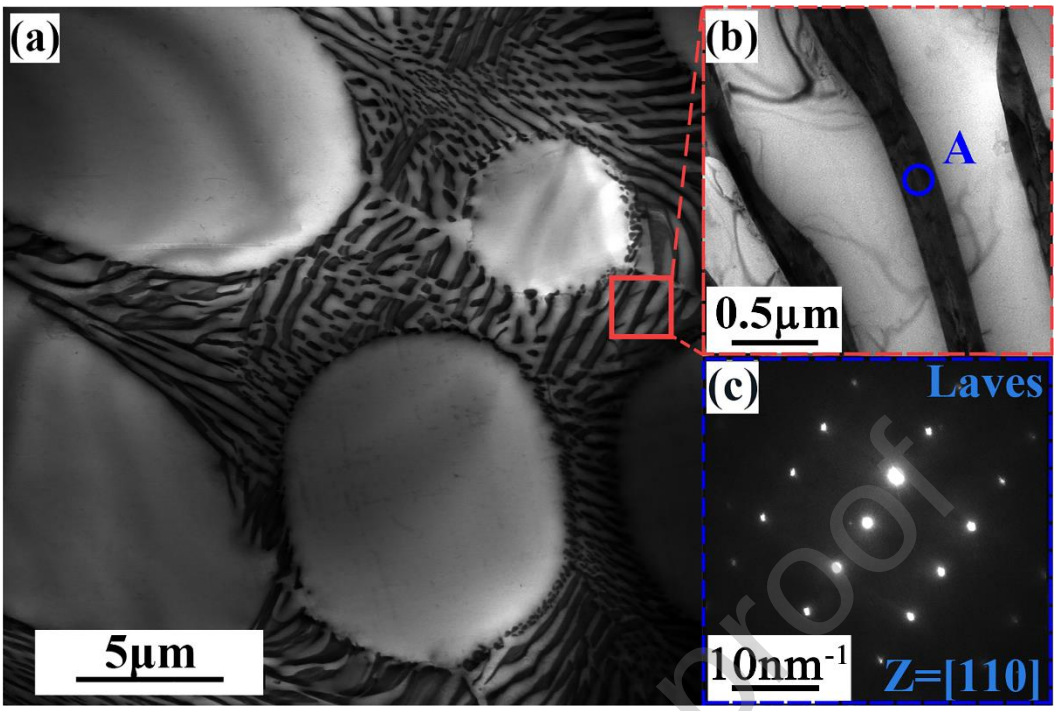

Fig. 3. TEM findings for $CoCrFeNiTa_{0.1}C_{0.1}$ HEA. (a) Bright field (BF) image. (b) Magnified depiction of the region enclosed by the red box in (a). (c) Corresponding selected area electron diffraction (SAED) pattern of region A in (b).

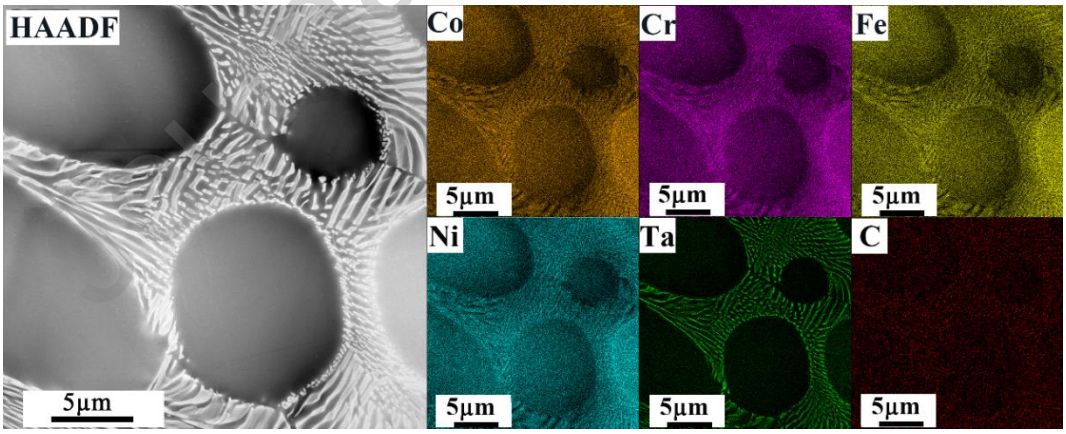

Fig. 4. The corresponding TEM-EDS mapping for $CoCrFeNiTa_{0.1}C_{0.1}$ HEA.

Table 2. The elemental contents of the individual phases within the $CoCrFeNiTa_{0.1}C_{0.1}$ HEA

Phase	Compositions (at.%)					
	Co	Cr	Fe	Ni	Ta	C
FCC	24.85±4.35	22.76±3.97	25.84±4.51	23.97±4.18	0.77±0.12	1.81±0.21
Laves	18.92±3.20	24.21±4.10	19.26±3.26	17.35±2.94	17.43±2.61	2.77±1.37

The BF images in Figs. 5(a-b) illustrates two distinct eutectic structures within the alloy, one manifesting as a composite of FCC and Laves phases and one as a combination of FCC and M_7C_3 carbide. Particularly intriguing that the discovery of a ternary eutectic structure in the area of the yellow box in Fig. 5(b). Fig. 5(c-d) shows the SAED pattern of the C0.1 alloy, further confirming that there are two distinct precipitates, the M_7C_3 carbide with hexagonal structure [35] and the Co_2Ta type Laves phase [36]. To determine the composition of these precipitates, elemental analysis of the ternary eutectic structure was performed, and the results are presented in Fig. 6. The EDS mapping displays a homogeneous dispersion of Co, Fe, and Ni elements within the matrix. In contrast, there is evident segregation of Cr, Ta, and C elements in the precipitates. Notably, the Ta element is prominently present in the bright precipitates. In combination with the XRD pattern, it is determined that the bright precipitate is the Ta-rich Laves phase. Additionally, a distinct enrichment of Cr and C elements is observed in carbide precipitates due to stronger atomic affinity resulting from negative mixing enthalpy between Cr and C atoms, exceeding that of other metal elements [37]. Consequently, it is determined that the lath precipitated phase is Cr-rich carbide. The specific element content of each phase is detailed in Table 3.

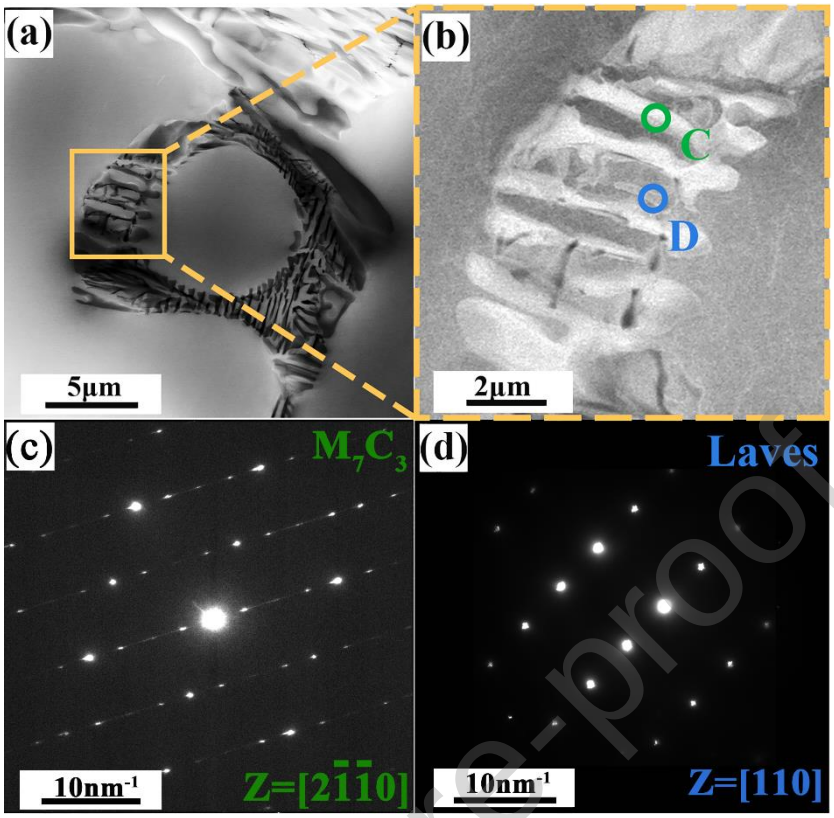

Fig. 5. TEM investigations of the $CoCrFeNiTa_{0.1}C_{0.3}$ HEA. (a) The BF images. (b) Enlarged image of yellow box area in (a). (c) The corresponding SAED patterns of the C region. (d) The corresponding SAED patterns of the D region.

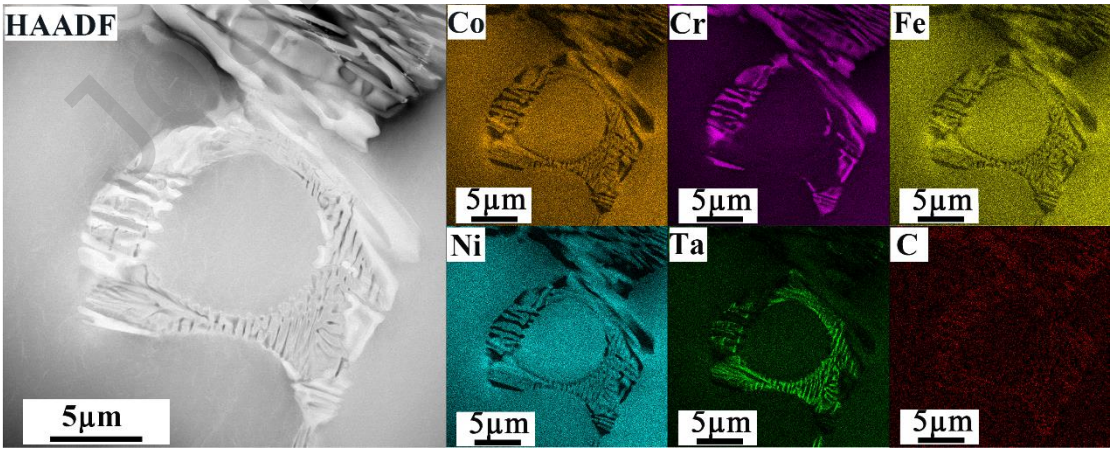

Fig. 6. The corresponding TEM-EDS mapping of $CoCrFeNiTa_{0.1}C_{0.3}$ HEA.

Table 3. The elemental components and contents of each phase within the

$CoCrFeNiTa_{0.1}C_{0.3}$ alloy.

Phase	Compositions (at.%)					
	Co	Cr	Fe	Ni	Ta	C
FCC	28.2±2.35	14.3±1.56	27.53±2.83	28.82±2.72	0.22±0.05	0.83±0.09
Laves	25.7±2.22	15.6±1.36	23.26±2.23	23.41±2.15	11.10±1.53	0.90±0.11
M_7C_3	16.7±2.03	50.72±1.2	18.67±1.95	11.78±1.48	0.34±0.03	1.72±0.29

Fig. 7 illustrates the TEM analysis of the C0.5 alloy. Fig. 7(a-b) shows that Laves phase content in the C0.5 alloy gradually decreases compared to the C0.3 alloy, and the ternary eutectic structure is no longer maintained. Furthermore, the carbide size and volume fraction increase with increasing C element content, as illustrated in Figs. 7(c-d). The STEM-EDS analysis of the C0.5 alloy is presented in Fig. 8. Similar to the C0.3 alloy, The Ta elements are enriched in the Laves phase and the C and Cr elements are enriched in M_7C_3 carbide. The amount of segregation of the Cr element in the alloy also increases as the C element increases. Table 4 provides the specific elemental composition of the C0.5 alloy.

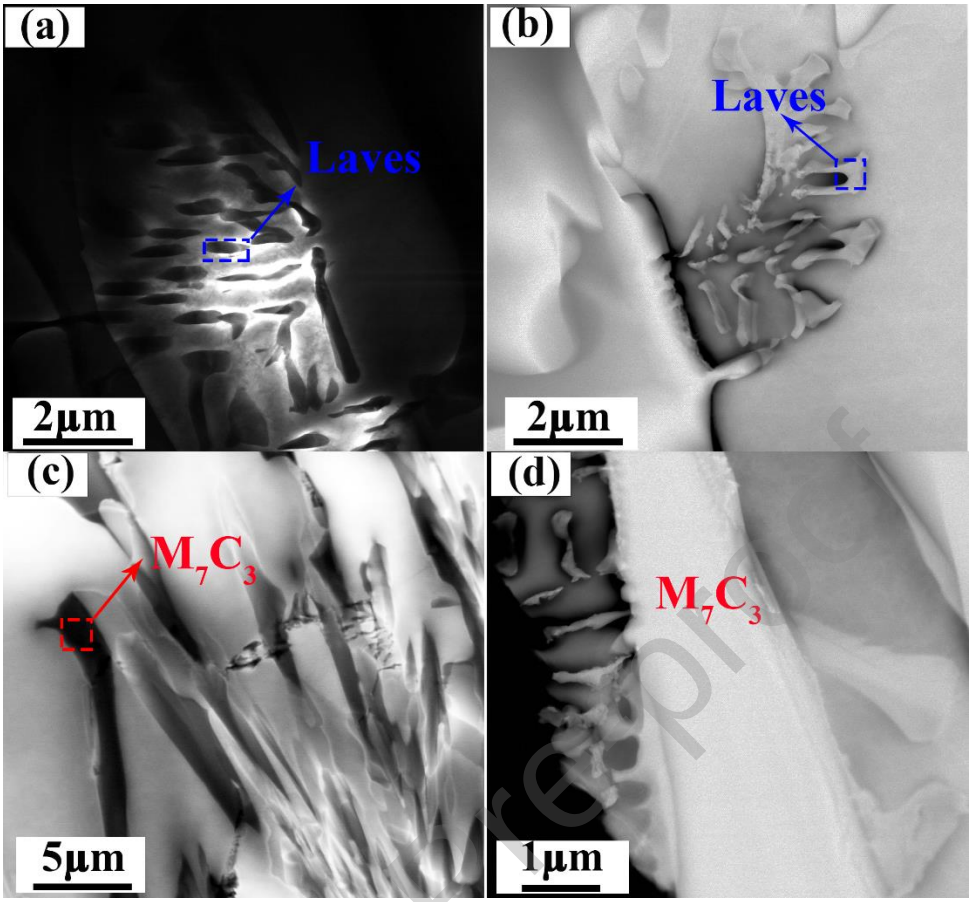

Fig. 7. TEM image of $CoCrFeNiTa_{0.1}C_{0.5}$ HEA.

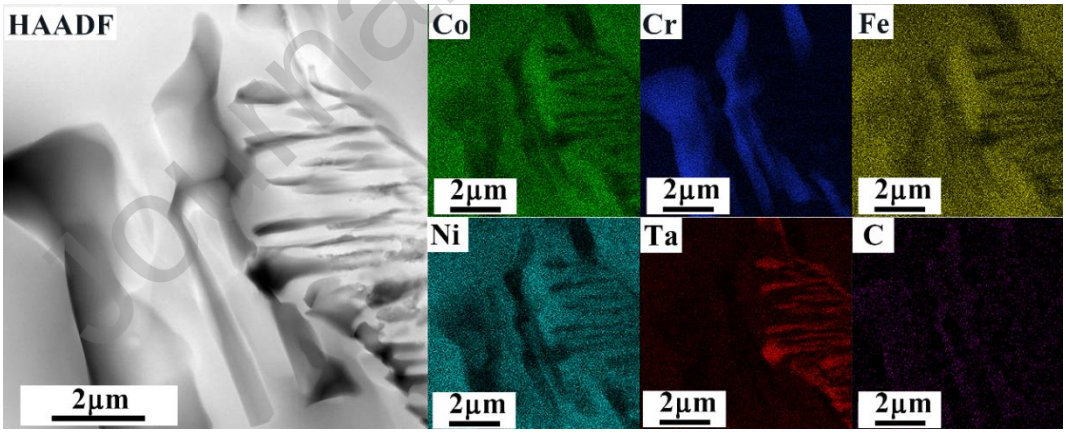

Fig. 8. The TEM-EDS mapping of $CoCrFeNiTa_{0.1}C_{0.5}$ HEA.

Table 4. The elemental components and contents of each phase within the $CoCrFeNiTa_{0.1}C_{0.5}$ alloy.

Phase	Compositions (at. %)					
	Co	Cr	Fe	Ni	Ta	C
FCC	28.69±4.9	14.4±2.55	27.8±5.04	28.4±5.14	0.15±0.04	0.56±0.10
Laves	22.9±3.83	16.9±2.82	21.1±3.52	20.0±3.34	14.55±2.15	4.51±0.97
M_7C_3	2.84±2.78	72.6±15.7	9.36±2.03	3.1±0.66	0.15±0.03	11.96±4.33

3.2 Macro-mechanical properties

Fig. 9(a) shows the compressive stress-strain curves of CoCrFeNiTa0.1Cx HEAs. The results indicate that the yield strength of C0 alloy is 307±11 MPa. The yield strength of the C0.1 alloy increases by 307±11 MPa to 649±15 MPa compared to the C0 alloy. The improvement in yield strength was mainly due to the generation of the Laves phase. It is worth noting that the C0, C0.1, C0.2, and C0.3 alloys did not fracture during the compression test, indicating excellent ductility. As C content increases, the yield strength of C0.2, C0.3, C0.4 and C0.5 alloys is 816±12 MPa, 1008±9 MPa, 1211±20 MPa and 1475±24 MPa, respectively. The precipitation of Laves phase and M_7C_3 carbide is the main reason for the increase of yield strength. Fig. 9(b) shows the Vickers hardness of the $CoCrFeNiTa_{0.1}C_x$ HEAs. The findings indicated that the hardness of the C0 alloy is 182±5 HV. As the C element content increases, the Vickers hardness of C0.1, C0.2, C0.3, C0.4 and C0.5 alloys at room temperature is 269±7 HV, 308±3 HV, 345±11 HV, 416±6 HV and 458±7 HV, respectively. As with the trend of yield strength, the Vickers hardness gradually increases with increasing C element content. The Vickers hardness, yield strength and ductility of the $CoCrFeNiTa_{0.1}C_x$

alloy are shown in Table 5.

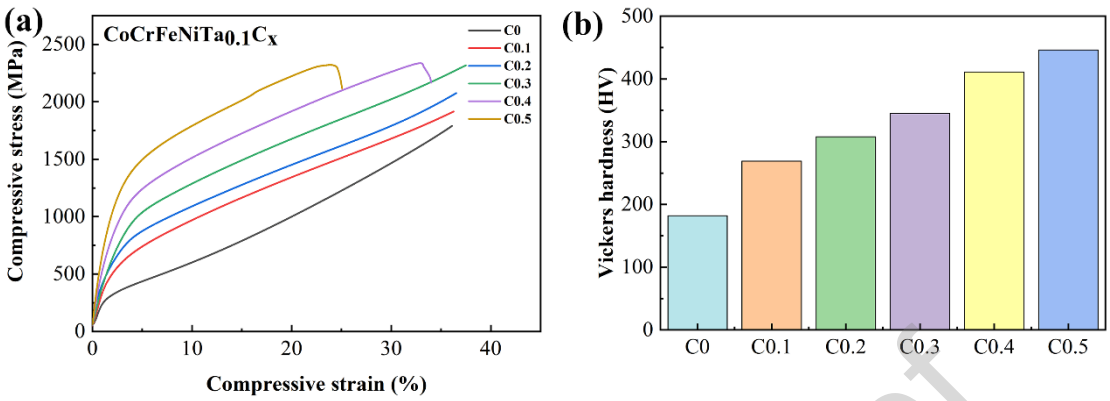

Fig. 9. The mechanical properties of $CoCrFeNiTa_{0.1}C_x$ HEAs. (a) Compression stress-strain curves. (b) Vickers hardness.

Table 5. The Vickers hardness (HV), yield strength (MPa) and ductility of $CoCrFeNiTa_{0.1}C_x$ HEAs

Alloys	Vickers hardness (HV)	Yield strength σ_y (MPa)	Ductility ε (%)
C0	182±5	307±11	Not fractured
C0.1	269±7	649±15	Not fractured
C0.2	308±3	816±12	Not fractured
C0.3	345±11	1008±9	Not fractured
C0.4	416±6	1211±20	33%
C0.5	458±7	1475±24	24%

3.3 Nano-mechanical behavior

Fig. 10(a) shows the typical load-displacement curves (*P-h*) in response to the indentation of the FCC phase, the Laves phase, and the M_7C_3 carbides of the C0.3 alloy.

The maximum penetration depths of the FCC and Laves phases were found to be ~185nm and ~205nm, respectively, significantly deeper than that of M_7C_3 carbides (~125 nm). This indicates that M_7C_3 carbides are harder than the FCC phase and Laves phase. The Oliver-Farr method [38] was employed to determine the nano-hardness and Young's modulus of the FCC matrix, Laves phase, and M_7C_3 carbides. The nano-hardness results in Fig. 10(b) display that the variations of the FCC phase and the Laves phase are not significant, measuring approximately 5.5 GPa and 7.7 GPa, respectively. However, with increasing C content, the nano-hardness of M7C3 carbide rises from 10.2 GPa to 18.5 GPa. Fig. 10(c) shows Young's modulus of the FCC phase, Laves phase, and M7C3 carbide are 202 GPa, 210 GPa, and 220 GPa, respectively. FCC alloys possess 12 slip systems, while HCP alloys have 3 slip systems. The more slip systems, the better the ductility [39]. Furthermore, the M_7C_3 carbide is a brittle phase and difficult to deform. Therefore, the presence of the Laves phase and M_7C_3 carbides increases the strength of $CoCrFeNiTa_{0.1}C_x$ HEAs, which consequently leads to a decrease in ductility.

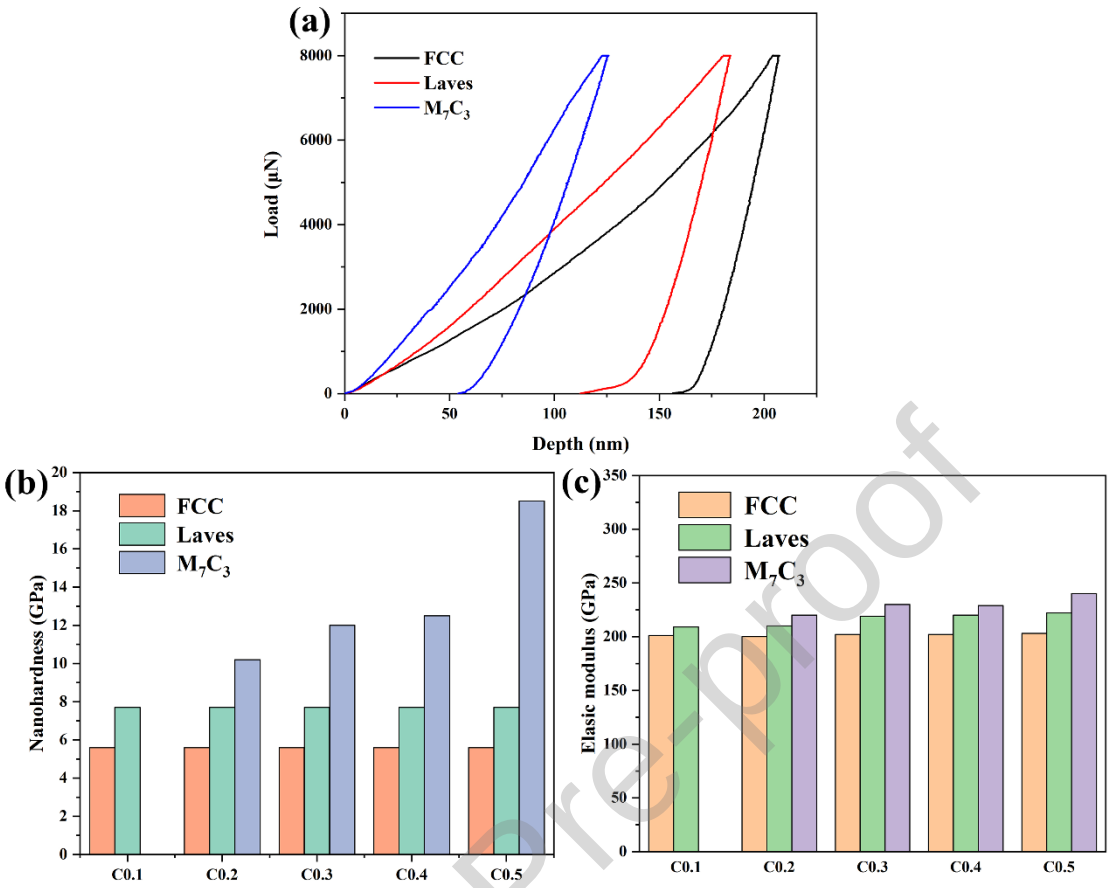

Fig. 10. (a) The typical load-displacement curves (*P-h*) of the FCC matrix, the Laves phase, and the M_7C_3 carbides nano-indentation within the C0.3 alloy. (b) The average nano-hardness values for various phases within the $CoCrFeNiTa_{0.1}C_x$ HEAs. (c) The average elastic modulus values for different phases within the $CoCrFeNiTa_{0.1}C_x$ HEAs.

4. Discussion

4.1 Effect of C additions on the phase selection of $CoCrFeNiTa_{0.1}C_x$ HEAs

Currently, there is no phase diagram available to accurately describe the phase composition and evolution of HEAs. Therefore, some simple phase formation criteria still play an important role in the field of HEAs. These criteria can be used to predict phase selection in alloys before conducting experiments. We chose to determine the

ability to form single-phase solid solution structures in HEAs using the geometric parameter (Λ) proposed by Singh et al. [40]:

$$\Lambda = \frac{\Delta S_{mix}}{\delta^2} \tag{2}$$

$$\delta = \sqrt{\sum_{i=1}^{n} c_i (1 - \frac{r_i}{\bar{r}})^2} \tag{3}$$

$$\Delta S_{mix} = -R \sum_{i=1}^{n} (c_i ln c_i) \tag{4}$$

$$\bar{r} = \sum_{i=1}^{n} c_i r_i \tag{5}$$

where ΔS_{mix} represents the mixing entropy of the alloy, δ denotes the atomic size mismatch, $r_{i,}$ and $\bar{r}$ are the atomic radii and the average atomic radius in the alloy c_i represents the atomic percentage of the *i*-th component, and *R* is the gas constant.

Criterion Λ states that when $\Lambda > 0.96$, the disordered solid solution phase tends to form in the alloy. Intermetallic compounds tend to form in alloys when $\Lambda < 0.24$. And when $0.24 < \Lambda < 0.96$, the multi-phase structure containing intermetallic compounds tends to form in the alloy [34]. The Λ values of $CoCrFeNiTa_{0.1}C_x$ HEAs are 0.46, 0.22, 0.15, 0.12, 0.09, and 0.08, respectively. The results show that the Λ values of C0.1, C0.2, C0.3, C0.4, and C0.5 alloys are all in the range of $\Lambda < 0.24$ and there are also intermetallic compounds in $CoCrFeNiTa_{0.1}C_x$ HEAs. Therefore, it can be shown that the Λ criterion is convenient for $CoCrFeNiTa_{0.1}C_x$ HEAs. Furthermore, by studying the influence of elements on the phase structure of the alloy, $\delta > 5$ has been proposed as an effective criterion for predicting the formation of the Laves phase [41]. The δ values of the $CoCrFeNiTa_{0.1}C_x$ alloy are 5.16, 7.59, 9.35, 10.76, 11.94, and 12.99, indicating the presence of Laves phase in all alloys. From the perspective of chemical compatibility, the possibility of phase formation in $CoCrFeNiTa_{0.1}C_x$ was evaluated

using electronegativity difference (Δx) as a characteristic parameter. The following formula can determine the electronegativity difference [42]:

$$\Delta x = \sqrt{\sum_{i=1}^{n} c_i (x_i - \bar{x})^2} \quad (6)$$

$$\bar{x} = \sum_{i=1}^{n} c_i \cdot x_i \quad (7)$$

where x_i stands for the Pauling electro-negativity of the *i*-th component, $\bar{x}$ represents the average Pauling electro-negativity. The Δx values of the $CoCrFeNiTa_{0.1}C_x$ alloy are 0.107, 0.156, 0.187, 0.213, 0.234, and 0.271, respectively. Wang et al. [43] indicate that when $\Delta x > 0.133$, it favors the formation of intermetallic compounds. For the $CoCrFeNiTa_{0.1}C_x$ alloy, in the absence of added carbon elements, the alloy predominantly exhibits a single-phase FCC structure. As the carbon content increases, there is a noticeable precipitation of the Laves phase and M_7C_3 carbides. The electronegativity of each constituent element can explain the variation in the content of the Laves phase and M_7C_3 carbides. With the addition of trace amounts of carbon, due to the lowest electronegativity of Ta, Ta preferentially precipitates to form the Laves phase with a $(Co/Cr/Fe)_2Ta$ structure. Consequently, as C content increases, only trace amounts of Ta element precipitate form the Laves phase, while more carbon combines with chromium to form high-content M_7C_3 carbides. This leads to an initial increase followed by a decrease in the content of the Laves phase with increasing carbon content, while the content of M_7C_3 carbides gradually increases.

4.2 Effect of C additions on macro-mechanical properties of $CoCrFeNiTa_{0.1}C_x$ HEAs

In the $CoCrFeNiTa_{0.1}C_x$ HEAs, the primary strengthening mechanism is precipitation strengthening. The volume fraction of the Laves phase and M_7C_3 carbides

directly influences the increase in yield strength (or hardness). The alloy's strength can be aptly described by a simple mixing rule, akin to conventional composites [44]:

$$\sigma_y = \sigma_{FCC}V_{FCC} + \sigma_{Laves}V_{Laves} + \sigma_{M7C3}V_{M7C3} \quad (8)$$

where σ_{FCC}, $\sigma_{Laves,}$ and σ_{M7C3} represent the yield strength of FCC, Laves phase and M_7C_3 carbides, V_{FCC}, $V_{Laves,}$ and V_{M7C3} denote volume fraction of the FCC, Laves phase and M_7C_3 carbides, respectively.

$$V_{FCC} + V_{Laves} + V_{M7C3} = 1 \quad (9)$$

Hence, the measured yield strength data for the C0.2, C0.3, C0.4, and C0.5 alloys are depicted as a function of V_{M7C3} in Fig. 11. The findings illustrate that the composite model effectively elucidates the observed increase in yield strength.

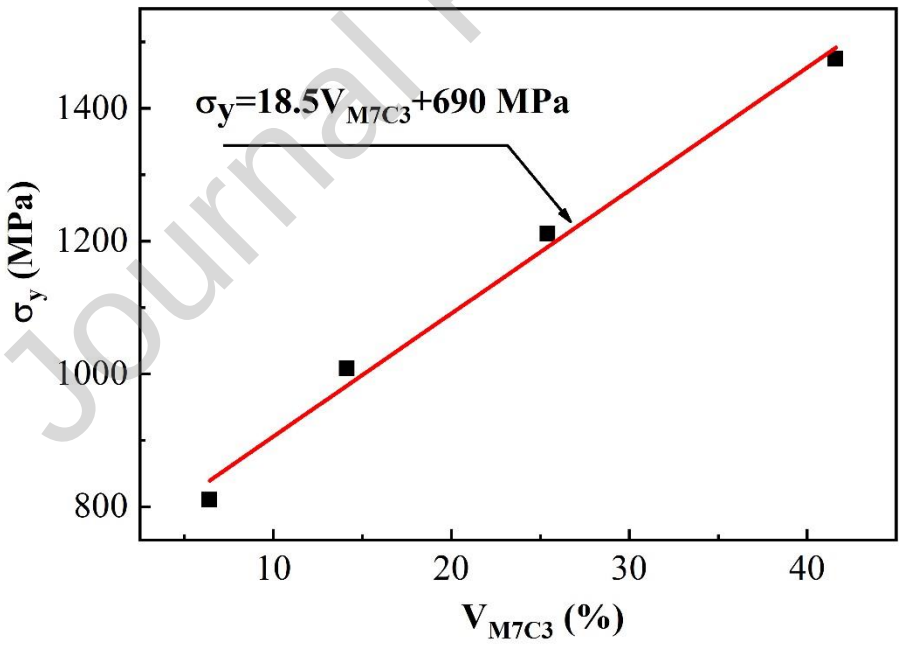

Fig. 11. The image demonstrates a nearly linear relationship between σ_y and V_{M7C3} for the C0.2, C0.3, C0.4, and C0.5 alloys.

4.3 Fracture mechanism

Fig. 12 presents the tensile fracture morphology of the C0.1 and C0.3 alloys at room temperature. In the C0.1 alloy, the presence of numerous dimples, as depicted in Figs. 12(a-a_1), signifies a fracture mode characteristic of ductile fracture. Figs 12(b-b_1) reveal that the C0.3 alloy exhibits a typical dendritic structure. The DR region displays evident dimples, indicating a ductile fracture mode. However, the ID region features intersecting river-like crack edges, suggesting a typical cleavage fracture in this region. Consequently, the fracture mode of the C0.3 alloy is identified as a mixed mode, encompassing both ductile and cleavage fracture characteristics. This observation indicates a transition in the fracture mechanism of $CoCrFeNiTa_{0.1}C_x$ HEAs from ductile to brittle as the C element content increases.

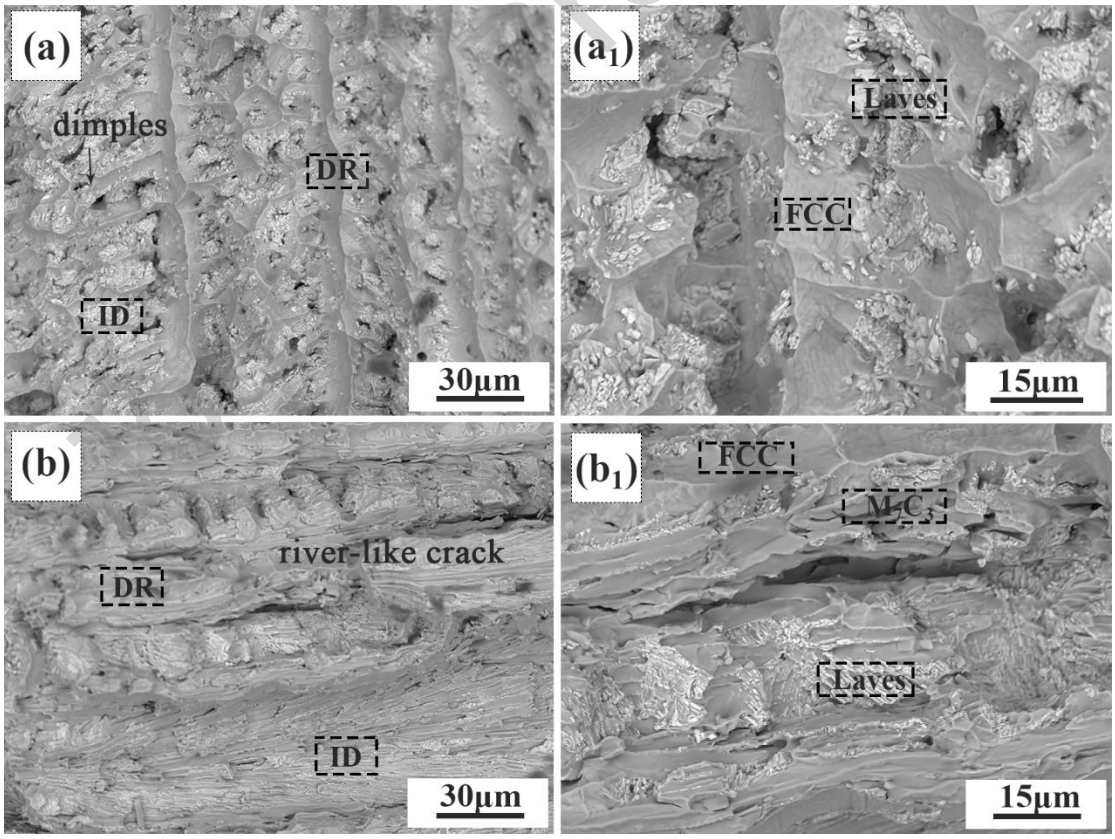

Fig. 12. The microstructure of the alloy after fracture. (a-a_1) The fracture morphology of C0.1 alloy. (b-b_1) The fracture morphology of C0.3 alloy

5. Conclusion

In this investigation, a series of $CoCrFeNiTa_{0.1}Cx$ HEAs with varying C content were successfully synthesized using vacuum arc melting technology. The study systematically analyzed the evolution of microstructure, mechanical properties, and fracture mechanisms of these alloys. By exploring the impact of carbon addition on the microstructure, valuable insights were gained into its role in modulating the microstructural characteristics. Microstructural analysis revealed a discernible pattern of initial augmentation succeeded by a subsequent decline in the Laves phase content within the alloys as the carbon content increased. Conversely, the content of M_7C_3 carbides exhibited a gradual increase. Moreover, in the $CoCrFeNiTa_{0.1}C_{0.3}$ alloy, a ternary eutectic structure was observed. Furthermore, the study meticulously investigated the influence of carbon content on the mechanical properties of the alloys, providing theoretical guidance for alloy design and optimization. Mechanical testing revealed a progressive enhancement in both the strength and hardness of the alloys with increasing carbon content, primarily attributed to the amplified volume fraction of brittle M_7C_3 carbides. These findings furnish crucial theoretical underpinnings for refining alloy preparation methodologies, exploring the intricate relationship between alloy microstructure and properties, and broadening the scope of applications in novel materials domains.

Acknowledgement

The Recipient of National Key R&D Program of China, Grant No: 2022YFA1603800 and the National Natural Science Foundation of China, Grant No. 12274362.

References

[1] B. Cantor, I.T.H. Chang, P. Knight, A.J.B. Vincent, Microstructural development in equiatomic multicomponent alloys, Mater. Sci. Eng. A 375-377 (2004) 213-218.

[2] S. Qin, M. Yang, P. Jiang, F. Yuan, X. Wu, Excellent tensile properties induced by heterogeneous grain structure and dual nanoprecipitates in high entropy alloys, Mater. Charact. 186 (2022) 111779.

[3] M. Slobodyan, E. Pesterev, A. Markov, Recent advances and outstanding challenges for implementation of high entropy alloys as structural materials, Mater. Today Comm. 36 (2023) 106422.

[4] J. Niu, Z. Fu, W. Chen, L. Hao, W. Xiong, T. Lu, H. Wen, Tailoring microstructure and tensile properties of low-cost AlCrFeNi-based high-entropy alloys via Co and/or Ti addition, Mater. Charact. 206 (2023) 113456.

[5] Y. Zhang, T.T. Zuo, Z. Tang, M.C. Gao, K.A. Dahmen, P.K. Liaw, Z.P. Lu, Microstructures and properties of high-entropy alloys, Prog. Mater. Sci. 61 (2014) 1-93.

[6] A.X. Li, P.F. Yu, Y.P. Gao, M.T. Dove, G. Li, Ultra-high strength and excellent ductility high entropy alloy induced by nano-lamellar precipitates and ultrafine grain structure, Mater. Sci. Eng. A 862 (2023) 144286.

[7] P. Chen, W. Wu, H. Liu, H. Li, C. Qiu, Metastable FeCrMnCo HEAs with the reinforcement of tungsten carbide fabricated by laser melting: Microstructure, mechanical properties and tribological behaviors, Mater. Charact. 206 (2023) 113397.

[8] H. Xu, Y. Xia, M. Chen, L. Ma, H. Li, B. Li, Z. Wu, X. Tan, Effect of Mo addition

on AC soft magnetic property, hardness and microstructure of FeCoNiMo ($0 \leq x \leq 0.25$) medium entropy alloys, Mater. Charact. 206 (2023) 113435.

[9] X. Fan, R. Li, X. Liu, Q. Liu, X. Tong, A. Li, S. Xu, H. Yang, P. Yu, G. Li, Synergistic strengthening of heterogeneous structures and dual-morphology nano-precipitates in Co1.5CrNi1.5Al0.2Ti0.1V0.1 medium-entropy alloy, Mater. Sci. Eng. A 832 (2022) 142492.

[10] X.H. Du, W.P. Li, H.T. Chang, T. Yang, G.S. Duan, B.L. Wu, J.C. Huang, F.R. Chen, C.T. Liu, W.S. Chuang, Y. Lu, M.L. Sui, E.W. Huang, Dual heterogeneous structures lead to ultrahigh strength and uniform ductility in a Co-Cr-Ni medium-entropy alloy, Nat. Commun. 11(1) (2020) 1-7.

[11] L. Fan, T. Yang, Y. Zhao, J. Luan, G. Zhou, H. Wang, Z. Jiao, C.T. Liu, Ultrahigh strength and ductility in newly developed materials with coherent nanolamellar architectures, Nat. Commun. 11(1) (2020) 1-8.

[12] J. Fan, X. Ji, L. Fu, J. Wang, S. Ma, Y. Sun, M. Wen, A. Shan, Achieving exceptional strength-ductility synergy in a complex-concentrated alloy via architected heterogeneous grains and nano-sized precipitates, Int. J. Plast. 157 (2022) 103398.

[13] Q. Wang, T. Zhang, Z. Jiao, J. Wang, D. Zhao, G. Wu, J. Qiao, P.K. Liaw, Z. Wang, Hierarchical precipitates facilitate the excellent strength-ductility synergy in a CoCrNi-based medium-entropy alloy, Mater. Sci. Eng. A 873 (2023) 145036.

[14] Z. Zhang, P. Jiang, F. Yuan, X. Wu, Enhanced tensile properties by heterogeneous grain structures and coherent precipitates in a CoCrNi-based medium entropy alloy, Mater. Sci. Eng. A 832 (2022) 142440.

[15] X.S. Liu, R. Li, X.F. Fan, Q.Q. Liu, X. Tong, A.X. Li, S. Xu, H. Yang, S.B. Yu, M.H. Jiang, C. Huo, P.F. Yu, M.T. Dove, G. Li, Excellent strength-ductility combination in Co36Cr15Fe18Ni18Al8Ti4Mo1 multi-principal element alloys by dual-morphology B2 precipitates strengthening, J. Mater. Sci. Technol. 134 (2023) 60-66.

[16] W. Lu, X. Luo, Y. Yang, K. Yan, B. Huang, P. Li, Nano-precipitates strengthened non-equiatomic medium-entropy alloy with outstanding tensile properties, Mater. Sci. Eng. A 780 (2020) 139218.

[17] B.X. Cao, H.J. Kong, Z.Y. Ding, S.W. Wu, J.H. Luan, Z.B. Jiao, J. Lu, C.T. Liu, T. Yang, A novel L12-strengthened multicomponent Co-rich high-entropy alloy with both high γ′-solvus temperature and superior high-temperature strength, Scr. Mater. 199 (2021) 113826.

[18] J. Man, B. Wu, G. Duan, L. Zhang, X. Du, Y. Liu, C. Esling, Super-high strength of a CoCrNiFe based high entropy alloy, J. Mater. Sci. Technol. 177 (2023) 79-84.

[19] D. Huang, Y. Zhuang, Break the strength-ductility trade-off in a transformation-induced plasticity high-entropy alloy reinforced with precipitation strengthening, J. Mater. Sci. Technol. 108 (2022) 125-132.

[20] X. Yang, L. Feng, T. Liu, R. Chen, G. Qin, S. Wu, Tensile properties and strengthening mechanisms of eutectic high-entropy alloys induced by heterostructure, Mater. Charact. 208 (2023) 113464.

[21] X. Liu, S. Zhang, H. Feng, J. Wang, P. Jiang, H. Li, F. Yuan, X. Wu, Outstanding fracture toughness combines gigapascal yield strength in an N-doped heterostructured medium-entropy alloy, Acta. Mater. 255 (2023) 119079.

[22] H. Kwon, P. Sathiyamoorthi, M.K. Gangaraju, A. Zargaran, J. Wang, Y.-U. Heo, S. Harjo, W. Gong, B.-J. Lee, H.S. Kim, High-density nanoprecipitates and phase reversion via maraging enable ultrastrong yet strain-hardenable medium-entropy alloy, Acta. Mater. 248 (2023) 118810.

[23] T.H. Chou, W.P. Li, H.W. Chang, B.X. Cao, J.H. Luan, J.C. Huang, T. Yang, Suppressing temperature-dependent embrittlement in high-strength medium-entropy alloy via hetero-grain/precipitation engineering, Scr. Mater. 229 (2023) 115377.

[24] J. Li, B. Gao, Y. Wang, X. Chen, Y. Xin, S. Tang, B. Liu, Y. Liu, M. Song, Microstructures and mechanical properties of nano carbides reinforced CoCrFeMnNi high entropy alloys, J. Alloys. Compd. 792 (2019) 170-179.

[25] Z. Lei, X. Liu, Y. Wu, H. Wang, S. Jiang, S. Wang, X. Hui, Y. Wu, B. Gault, P. Kontis, Enhanced strength and ductility in a high-entropy alloy via ordered oxygen complexes, Nature 563(7732) (2018) 546-550.

[26] W. Zhang, R. Liu, J. Liao, Z. Liao, R. Liu, K. Shi, Z. Yang, S. Qiu, J. Yang, Interface evolution and corrosion performance of (TiTaNbZrNi)N HEA coatings with a hybrid architecture under 6MeV Au-ion irradiation, J. Nucl. Mater. 567 (2022) 153832.

[27] L.J. Zhang, P.F. Yu, J.T. Fan, M.D. Zhang, C.Z. Zhang, H.Z. Cui, G. Li, Investigating the micro and nanomechanical properties of CoCrFeNi-Cx high-entropy alloys containing eutectic carbides, Mater. Sci. Eng., A 796 (2020) 140065.

[28] Y. Wang, X. Chen, X. Shi, Z. Xu, Y. Fan, L. Wang, Z. Chen, Investigation of microstructure evolution and mechanical properties of near-eutectic Fe2-yCoNiCryCx

high entropy cast iron, Intermetallics 154 (2023).

[29] S.R. Huang, J.F. Zhang, H.G. Zhu, Synergistic strengthening and toughening of eutectic C CoCr3Fe5Ni high entropy alloy, Transactions of Nonferrous Metals Society of China 34(4) (2024) 1204-1213.

[30] M. Klimova, D. Shaysultanov, A. Semenyuk, S. Zherebtsov, N. Stepanov, Effect of carbon on recrystallised microstructures and properties of CoCrFeMnNi-type high-entropy alloys, J. Alloys. Compd. 851 (2021) 156839.

[31] Z. Zhang, Y. Ling, J. Hui, F. Yang, X. Zhang, S. Tan, Z. Xie, F. Fang, Effect of C additions to the microstructure and wear behaviour of CoCrFeNi high-entropy alloy, Wear 530 (2023) 205032.

[32] H. Kotan, M. Tekin, A. Bayatlı, K.G. Bayrak, M. Kocabaş, E. Ayas, Effect of in-situ formed oxide and carbide phases on microstructure and corrosion behavior of Zr/Y doped CoCrFeNi high entropy alloys prepared by mechanical alloying and spark plasma sintering, Intermetallics 162 (2023) 107998.

[33] J.C. Alonso, O.C. Alonso, Derivation of unit cell volume, and lattice parameter of cubic high entropy alloys from volume size factors, Intermetallics 137 (2021) 107299.

[34] C. Ai, G. Wang, L. Liu, M. Guo, F. He, J. Zhou, Y. Chen, Z. Wang, B. Gan, Effect of Ta addition on solidification characteristics of CoCrFeNiTax eutectic high entropy alloys, Intermetallics 120 (2020) 106769.

[35] L. Zhang, P. Yu, J. Fan, M. Zhang, C. Zhang, H. Cui, G. Li, Investigating the micro and nanomechanical properties of CoCrFeNi-Cx high-entropy alloys containing eutectic carbides, Mater. Sci. Eng. A 796 (2020) 140065.

[36] H. Jiang, K. Han, D. Qiao, Y. Lu, Z. Cao, T. Li, Effects of Ta addition on the microstructures and mechanical properties of CoCrFeNi high entropy alloy, Mater. Chem. Phys. 210 (2018) 43-48.

[37] Y. Ma, X. Liu, W. Dong, R. Li, Y. Zhang, Y. Lu, P. Yu, G. Li, Interstitial carbide synergistically strengthening high-entropy alloy CoCrFeNiV0. 5Cx, Mater. Sci. Eng. A 792 (2020) 139802.

[38] W.C. Oliver, G.M. Pharr, An improved technique for determining hardness and elastic modulus using load and displacement sensing indentation experiments, Journal of materials research 7(6) (1992) 1564-1583.

[39] L. Zhang, P. Yu, M. Zhang, D. Liu, Z. Zhou, M. Ma, P. Liaw, G. Li, R. Liu, Microstructure and mechanical behaviors of GdxCoCrCuFeNi high-entropy alloys, Mater. Sci. Eng. A 707 (2017) 708-716.

[40] A.K. Singh, N. Kumar, A. Dwivedi, A. Subramaniam, A geometrical parameter for the formation of disordered solid solutions in multi-component alloys, Intermetallics 53 (2014) 112-119.

[41] H. Zhou, J. Mao, H. Jiang, H. Zhang, W. Wei, S. Qin, L. Tingjun, J. Xu, Effect of rare-earth element Y addition on microstructure and mechanical properties of CrFeNi2 medium entropy alloy, Intermetallics 163 (2023) 108079.

[42] X. Ji, Relative effect of electronegativity on formation of high entropy alloys, Int. J. Cast Met. Res. 28(4) (2015) 229-233.

[43] Y. Wang, X. Chen, X. Shi, Z. Xu, Y. Fan, L. Wang, Z. Chen, Investigation of microstructure evolution and mechanical properties of near-eutectic Fe2-yCoNiCryCx

high entropy cast iron, Intermetallics 154 (2023) 107805.

[44] J.Y. He, W.H. Liu, H. Wang, Y. Wu, X.J. Liu, T.G. Nieh, Z.P. Lu, Effects of Al addition on structural evolution and tensile properties of the FeCoNiCrMn high-entropy alloy system, Acta. Mater. 62 (2014) 105-113.

Conflict of Interest

All authors have read and approved this version of the article, and due care has been taken to ensure the integrity of the work. No part of this paper has been published or submitted elsewhere. No conflict of interest exists in the submission of this manuscript.

Highlight

- With the addition of C element, Laves phase and M_7C_3 carbides gradually appear in the alloys and form two eutectic structures (FCC+Laves and FCC+M_7C_3).
- As the C element increases, the volume fraction of M_7C_3 carbide increases while the volume fraction of Laves phase decreases.
- Ternary eutectic structure can be observed as the C element increases.